Sustainable Materials and Technologies 33 (2022) e00486

Contents lists available at ScienceDirect

Sustainable Materials and Technologies

journal homepage: www.elsevier.com/locate/susmat

Circular solid state reduction process of fine copper powder synthesis with life cycle assessment for photovoltaics application

Filip Cebula [a], Konrad Wojtaszek [a], Hasan Shabbir [a], Anna Kula [a], Zbigniew Pędzich [a], Kamil Kornaus [a], Stanisław Małecki [a], Karolina Kołczyk-Siedlecka [a], Robert P. Socha [b], Marc Escribà-Gelonch [c], Katarzyna Rogóż [d], Michael Goodsite [e], Volker Hessel [f,g], Marek Wojnicki [a,b,*]

[a] AGH University of Science and Technology, Mickiewicza Ave. 30, 30-059 Krakow, Poland
[b] Research and Development Center of Technology for Industry, Ludwika Waryńskiego 3A, 00-645 Warszawa, Poland
[c] University of Lleida, Department of Chemistry, Higher Polytechnic Engineering School, Igualada, Spain
[d] KGHM Polska Miedź S.A., Poland
[e] The University of Adelaide, Institute for Sustainability, Energy and Resources Division of Research and Innovation, Adelaide, Australia
[f] School of Engineering, University of Warwick, UK, United Kingdom
[g] The University of Adelaide, School of Chemical Engineering and Advanced Materials, Adelaide, Australia

ARTICLE INFO

Keywords:
Copper powder
Synthesis
Pyrometallurgy
Life cycle assessment
Circularity

ABSTRACT

This paper presents the process of synthesis of copper powders obtained by the pyrometallurgical method without the participation of the liquid phase. This method is based on the simultaneous decomposition and reduction of copper (II) carbonate. Hydrogen was used as a reducing agent. Due to the strongly exothermic thermal effect of the reduction reaction, a mixture of inert gas and hydrogen was used to better control the parameters. Studies have shown that the carbonate method enables the synthesis of copper powders with a narrow distribution and controlled size. The size is controlled by the grinding time of the copper (II) carbonate. An life cycle assessment and circularity study evaluate the sustainability of the new process, and focus is given to the energy efficiency.

1. Introduction

1.1. The importance of copper-base powder

Copper-base powder metallurgy products rank third after iron/steel and aluminum-based powder-making (PM) products in terms of volume [1]. The main applications are oil bearings, friction materials, diamond tools, thermal conductivity and contact materials, and chemical catalysts [2]. Vishnu K Mohan et al. [3] reported that copper powder can increase the tensile strength up to 18.55% for Friction Stir Welding. Another research by Cynthia Samuel Abima et al. [4] reported the effect of copper on MIG welding of aluminum. They reported the inclusion of copper powder to increase the hardness values both in the fusion zone and in the heat-affected zone by forming intermetallic compounds. The copper powder also improves the grain structure in the aluminum weld which improves corrosion resistance. Copper powder can also help to improve the mechanical properties of metals. Jituo Liu et al. [5] reported that Ni-doped graphene matrix when prepared with copper powder enhances the yield strength, hardness, and conductivity of the matrix. It was shown that copper can improve the fatigue threshold of porous steel by forming intermetallic compounds. Setuo Takaki et al. [6] reported that copper addition to steel improves the strength-ductility ratio, when compared to copper-free steel, by forming fine ferrite grains, which are generally lower than 1 μm. The copper powder can also positively influence thermal properties [7]. It was reported that nylon-based composites show good thermal conductivity when copper is used in them [8]. The rising role of additive manufacturing caused an increasing demand for metal powders [9–11], and many studies have shown how the quality of the powders impacts the process [12–14].

Photovoltaics is one of the fastest and most dynamically developing industries. Recent studies indicate the great potential importance of copper powders in this area [15,16]. The copper powder can be used as a

* Corresponding author at: AGH University of Science and Technology, Mickiewicza Ave. 30, 30-059 Krakow, Poland.
E-mail address: marekw@agh.edu.pl (M. Wojnicki).

https://doi.org/10.1016/j.susmat.2022.e00486
Received 20 April 2022; Received in revised form 11 August 2022; Accepted 26 August 2022
Available online 1 September 2022
2214-9937/© 2022 The Authors. Published by Elsevier B.V. This is an open access article under the CC BY-NC-ND license (http://creativecommons.org/licenses/by-nc-nd/4.0/).

screen print paste used in a high-temperature metallization process [17] to fabricate the front contacts of Si solar cells. Thanks to this, it is possible to significantly reduce the cost of production. It is worth noting that silver is about 50–150 times more expensive than copper [18]. Nowadays, the cost of silver in photovoltaics panels is estimated to be 1.1 USD cent/Wp power [19]. To show the importance of this technology more vividly, silver paste is 14% of the production cost [20]. Therefore, an effort is made to replace silver with copper in electrically conductive pastes. Piotr Panek et al. [21] successfully reduced the consumption of silver in printing pastes, by adding a copper composite obtained by chemical treatment of copper powder to a commercial silver print paste. The result was a mixture of 50% of commercial silver paste and 50% copper composite. The solar cell produced with the use of this paste achieved the best result ever obtained concerning direct Cu application for solar cells fabricated in thick-film technology at that time. The development of nanoparticle copper screen printing pastes for silicon heterojunction solar cells was a topic studied by Boon Heng Teo et al. [22]. In this paper copper printing pastes with various amounts of copper were evaluated in terms of printability, line resistance, and contact formation to Indium-Tin Oxide (ITO) transparent conductive oxide layers. The authors note that the specific contact resistivity of the Cu paste is comparable to state-of-the-art Ag pastes used in high-efficiency HJ cells.

Taking into consideration all listed applications and the constant development of electronics, one can only predict the increasing demand for copper powders.

1.2. Synthesis of copper powders

The synthesis of copper powders can be carried out in many ways. The main methods of production can be divided into four groups [1]: atomization, electrolysis, solid-state reduction, and hydrometallurgy.

The electrochemical method is very popular, mainly due to its simplicity. It has already been very well developed [23–25], unfortunately, due to the necessity to conduct the process under diffusion control conditions, the electrical efficiency of this process is quite low [26,27]. There are many studies on the possibility of changing the electrolyte composition in order to improve efficiency [28]. The general tendency is maintained, which indicates, that the production of very fine copper powders (<10 μm) requires the consumption of much more electricity than the production of copper powders <100 μm [29]. This is due to the parallel reaction associated with the evolution of hydrogen [30]. Size for commercially available electrolytic copper powder ranges between 45 and 106 μm [31,32], fine powder is estimated around 4–10 μm [33], and nanopowder 35–60 nm [34]. Obtained powders usually have dendritic morphology, which can be a disadvantage in some processes like powder injection molding [35]. Zhang et al. [2] report that power consumption to manufacture electrolytic copper powder ranges between 3800 and 4200 kWh t^{-1}. Although Xia et al. [36] report, that power consumption in this process can be as low as 719 kWh t^{-1} for copper powder with a particle size of 47 nm.

Other methods of synthesizing copper powders are based on the chemical reduction of copper (II) ions to a metallic form [37,38]. This method offers powders with good dispersibility [39], recycling of metal scraps, spent electrolytes, industrial wastewater [40], and a wide variety of possible products [41,42]. Unfortunately, these methods are frequently not environmentally benign [43]. The use of green reducers reduces this burden, but the amount of liquid waste generated is significant. Agraval et al. [44] also report challenges involving the agglomeration of particles and the plating of metal on the interior walls of the reactor.

At present, the atomization process is very often used on an industrial scale [31–33,45]. This method consists of copper melting and then spraying it in inert gas or water, which is both a cooling and atomizing agent. This method gives very good results [46,47]. By controlling the temperature of the liquid copper, choosing an atomizing agent, the gas or liquid flow rate, and the shape and parameters of the atomizer, it is possible to control the particle size [48–50]. Just by changing feedstock and adjustment of parameters, various alloys and metals can be produced with the use of the same system. Relevant problems with the atomization method are Freeze-up's, or furnace melt solidification [51]. After the metal has been melted and poured into the tundish, the molten alloy begins to lose heat rapidly. The alloy can solidify and create build-up in the atomization nozzle, causing a blockage or “freeze-up”, which creates the need to stop production for cleaning the machine [52]. Obtained powder is characterized by wide particle size distribution, which means a lower quantity of specific powder size. The low yield of atomized powder between 20 μm and 150 μm is still an important issue [9]. Zhang et al. [2] report that power consumption to manufacture atomized copper and copper alloy powder equals 2000 kWh t^{-1}.

In solid-state reduction, cupric oxide powder is reduced by a gas, usually hydrogen, carbon monoxide, or cracked natural gas, at a temperature below the melting point of copper [53,54]. The size of powder particles obtained by this method is controlled by the size of the used oxide [55]. The main advantage is the low cost of this method and efficient production [56,57], and the large specific surface area of produced powders [58]. Unfortunately, this method produces a lot of green gas products. The purity of obtained powder is not controlled during the process, and it depends on the purity of the precursor. That is why obtained powder can have lower purity compared to other methods.

Often, an additional milling process is needed to obtain a specific size of the copper powder. This process allows for reducing the particle size of a fraction that did not meet expectations. It is important to point out, that due to the plasticity of copper, morphology will change to plate-like and/or flaky [59,60]. The biggest disadvantage of this process is low energy efficiency [61]. To effectively reduce the size of the malleable powder, the material must be sufficiently saturated with dislocations until it becomes brittle and fractures [62]. For this reason, milling copper powder requires significantly more energy than grinding brittle materials.

Therefore, work was undertaken to use a method based on the already known processes of powder synthesis, but with particular emphasis on thermodynamics and process kinetics, in order to estimate the energy gain of hybrid methods of copper powder synthesis. We propose the concept of technology that allows the green production of copper powder. The main process combines the well-known thermal decomposition of copper carbonate [63,64] and hydrogen reduction of copper oxide into a simple and efficient solid-state reduction method. With the incorporation of well-known and used in industry reactions, the zero-emission, close cycle technology can be achieved.

2. Experimental

Copper carbonate was obtained in our laboratory. For this purpose, copper (II) nitrate (POCH, analytical pure) was dissolved in deionized water (Polwater DL3N-150). An aqueous sodium carbonate (Sigma-Aldritch, analytical pure) solution was then added. As a result of the double exchange reaction, copper carbonate was obtained in the form of a fine powder.

The solution was then filtered, rinsed, and dried in a laboratory (SML-32/250) drier for 48 h at 100 °C.

The grinding processes were carried out in a commercial grinder (dedicated to grinding coffee, DeLonghi KG200). Different milling times were used to obtain different copper carbonate powders.

The processes of reduction and decomposition of copper carbonate were carried out in a tube furnace. The tube of the furnace was made of quartz. The samples were placed in containers also made of quartz, cylindrical in shape, 2 cm in diameter, and 2 cm in height.

A commercial 5/95% H_2/Ar gas mixture with 99.999% purity was used as a reducing agent (Airliqiud, Poland).

The samples were placed in the geometric center of the furnace to ensure equal temperature distribution. The furnace was controlled by a

PIV controller.

Several techniques were used to analyze the size of the copper powders and copper (II) carbonate. Electron microscopy SEM (Hitachi SU-70), and laser diffraction particle size analyzer (Mastersizer 2000) were used. In order to ensure SEM charge-free imaging, copper (II) carbonate particles and copper powders were coated with a thin gold or carbon layers by using the K575XD Turbo Pumped High-Resolution Sputter Coater and the Cressington 208 carbon coater. Before measurements using Mastersizer instruments, the samples were dispersed in deionized water. For this purpose, the ultrasonic head (Sonic & Materials, vibra cell) was applied for 3 min, with an applied amplitude of 40%.

The crystal structure was determined by XRD analysis, using a Rigaku Miniflex II X-ray diffractometer with Cu-Kβ (30 kV, 15 mA, k = 1.5406 Å) radiation and scanning angles between 20^0 and 90^0. Williamson-Hall method was used to calculate the size of the crystallites. The analysis was performed for powder reduced in temperature equal to 300 °C.

XRF analysis was used to characterize the purity of the obtained powders. For this purpose, the ED-XRF: Bruker, model: S2 Puma was used. Elemental composition measurements were made in the air using the Smart-Elements method in fashion without the use of a calibration curve (Standardless). Before starting the measurements, the device was calibrated according to the manufacturer's procedure. The reference values for the standard used for the check (QC sample) were consistent with the values declared by the manufacturer. The normalization procedure was used to determine the content of individual elements. Due to the signal from silicon observed in the sample (most likely resulting from SiO_2 sample holder), the results of the analysis were calculated disregarding the silicon content. The test was performed for powder reduced in temperature equal to 300 °C.

Differential Thermal Analysis and Differential Scanning Calorimetry, DTA-DSC, was used for the characterization process of copper powder synthesis, using TA Instruments SDT Q.600. Thermal analyses of the aforementioned materials were conducted in the H_2/Ar atmosphere, with the flow of the gas equal to 100 mL/min unless otherwise stated.

The surface area of the copper powder was determined with the Brunauer–Emmett–Teller (BET) method (Micromeritics ASAP 2010). The sample before measurements were degaussed for 24 h at the temperature of 150 °C. Nitrogen gas was used as the adsorbate, assuming that a single nitrogen molecule can cover 0.16 nm^2 of the substrate area. Additionally, BET measurements were carried out to verify whether the obtained materials were solid or porous.

The conductivity test of obtained copper powders was performed specially for this purpose system, based on assembly presented by Juan et al. [65]. For resistance measurement, the Keithley 2000 Series: 6.5 Digit Multimeter was used. The experiment consisted of 10 measurements of resistivity under different pressures. The test was performed for powder reduced in temperature equal to 300 °C.

3. Results and discussion

The technology design requires a series of steps to finally succeed. Typically some steps have to be repeated, to solve specific sub-problems. The first step is related to the identification of the problem to solve. In our case, we analyze the demand of the market dealing with the production of photovoltaic panels that need appropriate soldering pastes. Leaving aside the details, the problem is the need to lower the production costs of copper powders, in order to maintain their properties, i.e. grain size below 5 μm. There are many technologies for the production of powders, but some of them do not give the product with the required properties. Specifying the maximum size of the powder (5 μm) causes a sharp increase in production costs. It is observed at the stage of offering and purchasing copper powders. Therefore, based on the experience of our own and cooperating units, we undertook research on the development of new technology for their production, based on already known and working sub-technologies. The technology concept is described in detail in Section 3.1.

The next step of the technology design is proof of concept on the laboratory scale. In our opinion, the key step is the proper selection of the parameters of the reaction of copper carbonate to copper powder. This implies a series of related experiments described below. The last key element of technology design is to determine the cost of the technology and its impact on the environment. Therefore, a detailed analysis of the sustainability metrics is also carried out.

3.1. Technology concept

As presented in the introduction section, there are many ways to produce copper powders. The use of spray methods consumes a huge amount of energy, whereas the use of chemical methods generates large amounts of wastewater. We propose a sustainable thermal and chemical system for the production of copper powders. The process scheme is shown in Fig. 1. The key idea is to propose recycling processes in order to regenerate the raw materials before feeding them back. Yet, the risk is that these parallel processes are prone to generate secondary wastes, which could finally reduce their benefits and have an environmental impact. (See Table 1.)

As start-up reactions the following processes are required:

$$3HNO_3 + Cu_{bulk} = Cu(NO_3)_2 + NO_x + \frac{3}{2}H_2O \quad (1)$$

Next, obtained copper(II) nitrate can be used to obtain copper(II) carbonate:

$$Cu(NO_3)_2 + K_2CO_3 \xrightarrow{H_2O} CuCO_3 + 2KNO_3 \quad (2)$$

The reaction (1) is well known and fast. However, the generated gases required more sophisticated technology to be utilized. Therefore the reactions (1) and (2) can be substituted by slower, however, more environmentally benign one.

$$Cu_{bulk} + H_2SO_4 + \frac{1}{2}O_2 \xrightarrow{H_2O} CuSO_4 + H_2O \quad (3)$$

and

$$CuSO_4 + K_2CO_3 \xrightarrow{H_2O} CuCO_3 + K_2SO_4 \quad (4)$$

The reaction (3) is also used on an industrial scale although its application is limited by the low reaction rate.

In the presented system, only electricity is consumed. Water is used to produce hydrogen (reducing agent). The carbon dioxide needed to make the carbonate is circulated throughout the system, and other salts are effectively used in a closed cycle.

By using the waste heat from each stage, it is possible to increase the efficiency of the entire system. Assuming that the plant works on the green energy principle, it is possible to produce copper powders without a lasting negative impact on the environment.

The experimental study in this paper has been focused on one stage (central reaction in Fig. 1) of this technology concept. According to our assessment, it is the key reaction for this technology, whereas the rest of the reactions are already implemented in the industry or have good application potential.

.

Initial thermodynamic calculations related to the decomposition of copper carbonate and the reduction of copper oxide to metallic copper were carried out.

Thermodynamic calculations are very helpful; unfortunately, they say nothing about kinetics, so experimental work is also required. Three reactions are dominating in the system. The first one direct reduction of copper(II) carbonate do metallic form by hydrogen (see eq. (5)). Probably in parallel, the process of copper(II) carbonate decomposition to copper(II) oxide takes place (see Eq. (6)). Next, the copper(II) oxide is

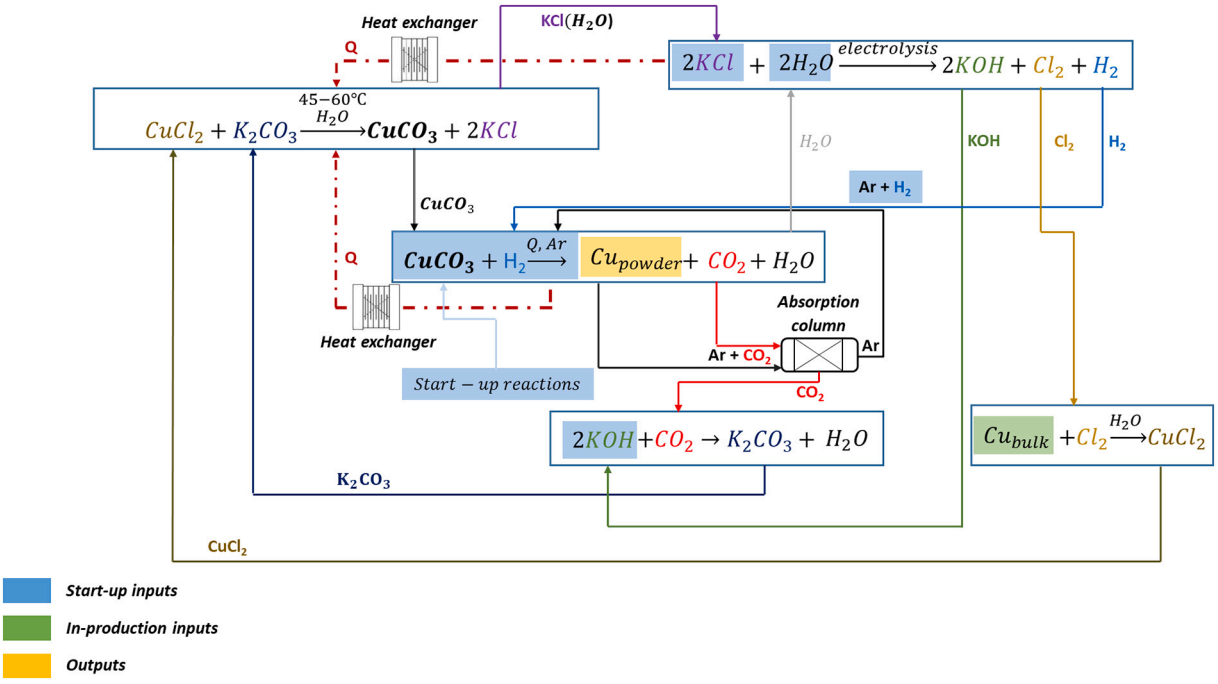

Fig. 1. Concept of zero waste technology connected with Life Cycle Assessment inventory.

Table 1
Characterization of main production methods of copper powder.

	Atomization	Electrolysis	Hydrometallurgy	Solid state reduction
Advantages	Low production cost	Simplicity	Recycling	Low cost
	Suitable for large-scale production	Particle size ranges from a few nanometers to several millimeters	Excellent dispersibility	Efficient production
	Can be used for various types of alloys and metals	Good compressibility	Possibility to produce various products	Large specific surface area
Disadvantages	Low yield of powder between 20 and 150 μm	Power consumption (High cost)	Secondary wastewater	Lowest purity of all methods (98–99%)
	"Freeze-up's" (Furnace melt solidification)	Poor packing and rheology in the molding process	Agglomeration of particles	Green gas by-products
	Wide particle size distribution	The process demands purification so that residual impurities could be removed	Plating of metal of the interior wall of reactor/internal fittings	

reduced by hydrogen to metallic copper (see Eq. (7)).

$$CuCO_3 + H_2 \underset{\leftarrow}{\rightarrow} Cu + H_2O + CO_2 \quad (5)$$

$$CuCO_3 \rightleftarrows CuO + CO_2 \quad (6)$$

$$CuO + H_2 \underset{\leftarrow}{\rightarrow} Cu + H_2O \quad (7)$$

As it can be calculated (see Fig. 2), all shown above reactions have negative Gibbs free energy (ΔG). This indicates that they can occur simultaneously.

The reaction (5) and the reaction (7) are strongly exothermic, while the reaction (6) is endothermic. The uncontrolled increase in temperature leads to the sintering of the copper powder particles. As a result, the obtained powders are of poor quality. Therefore, the tests were carried out with the use of a mixture of 95% Ar and 5% H_2. As a result, the speed of the reduction reaction is much slower than in comparison to the system where pure hydrogen is used. It is further emphasized that, in this particular case, the rate of heat removal from the reaction area is mainly controlled by the flow rate of the gases. Gases have a low heat conductivity coefficient and low heat capacity, which additionally makes it difficult to properly control the process. DTA measurements were carried out to determine the temperature range in which the reduction reaction dominates (a mixture of 5% H_2 and 95% Ar was introduced into the system) and the reaction of copper (II) carbonate decomposition (Ar was pumped into the system). Obtained results are shown in Fig. 3.

As it can be seen, in the case where the mixture of 95% Ar and 5% H_2 are pumped into the systems, two picks are observed. The first one is endothermic, and the second one is exothermic. At first, the endothermic reaction takes place. It is observed that these two peaks are partially overlapping (see Fig. 3. A). Thanks to that, energy consumption in the process is lower.

3.2. Process rate studies

The rate of mass loss is the measurement of the reaction rate, as well as the rate of energy release/consumption in the process. The results of the amusements are presented below (see Fig. 4). The dashed red lines show the speed of the two reactions (6) steps.

Under experimental conditions (continuous gas flow), the reaction (6) can be written as:

$$CuCO_3 \xrightarrow{k_1} CuO + CO_2 \quad (8)$$

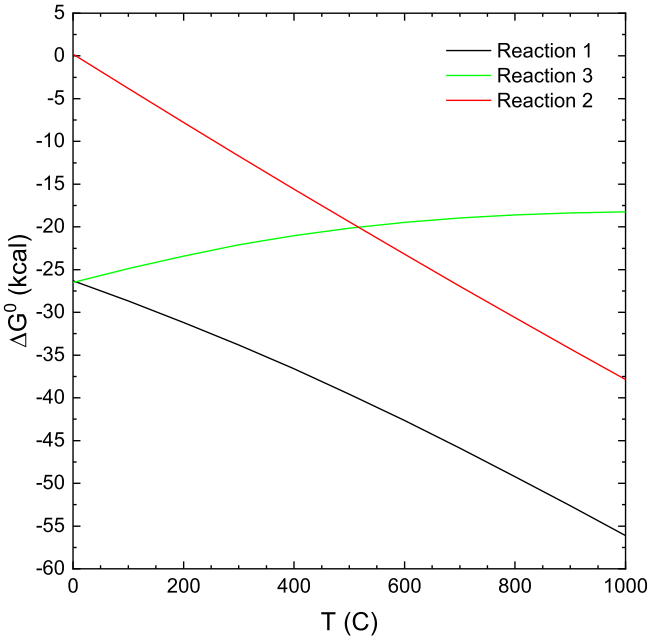

Fig. 2. Thermodynamic calculations of Gibbs free energy for the reactions taking place in the system.

and the reaction (7) can be written as:

$$CuO + H_2 \xrightarrow{k_2} Cu + H_2O \tag{9}$$

where k_1 and k_2 denote reactions rates, the shape of the kinetic curves (see Fig. 4) suggests that the order of the reaction is zero. Therefore, the velocity of the reaction can be written as:

$$V_1 = -\frac{d[CuCO_3]}{dt} = k_1 \tag{10}$$

$$V_2 = -\frac{d[CuO]}{dt} = k_2 \tag{11}$$

From the experimental data shown in Fig. 4, reaction rate constants were determined. Obtained values are shown in Table 2.

It can be seen that in the case of the experiments carried out above 210 °C, there are no changes in the reaction rate for the first reaction. This suggests that above this temperature the process is controlled by mass transport (CO_2) from the copper (II) carbonate surface. However, below this temperature, the process is activation controlled or in the range of mixed control. Clearing this uncertainty requires a detailed study of the mechanism, which is not the subject of this work. However,

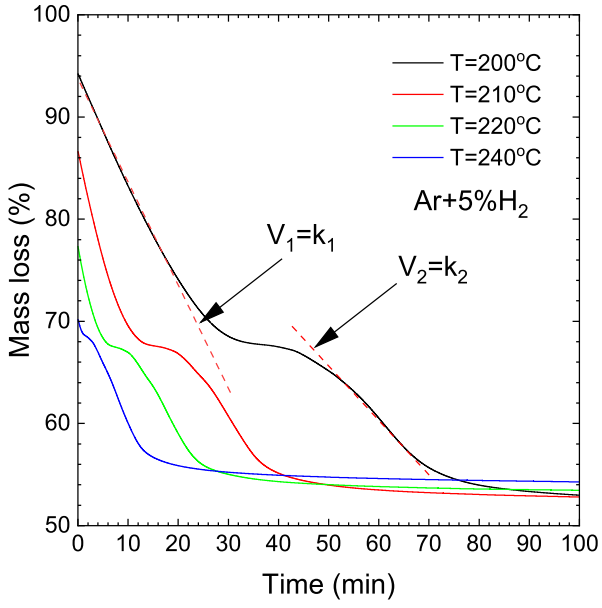

Fig. 4. Influence of experimental temperature on the process rate. Experimental conditions: gas flow 100 mL/min.

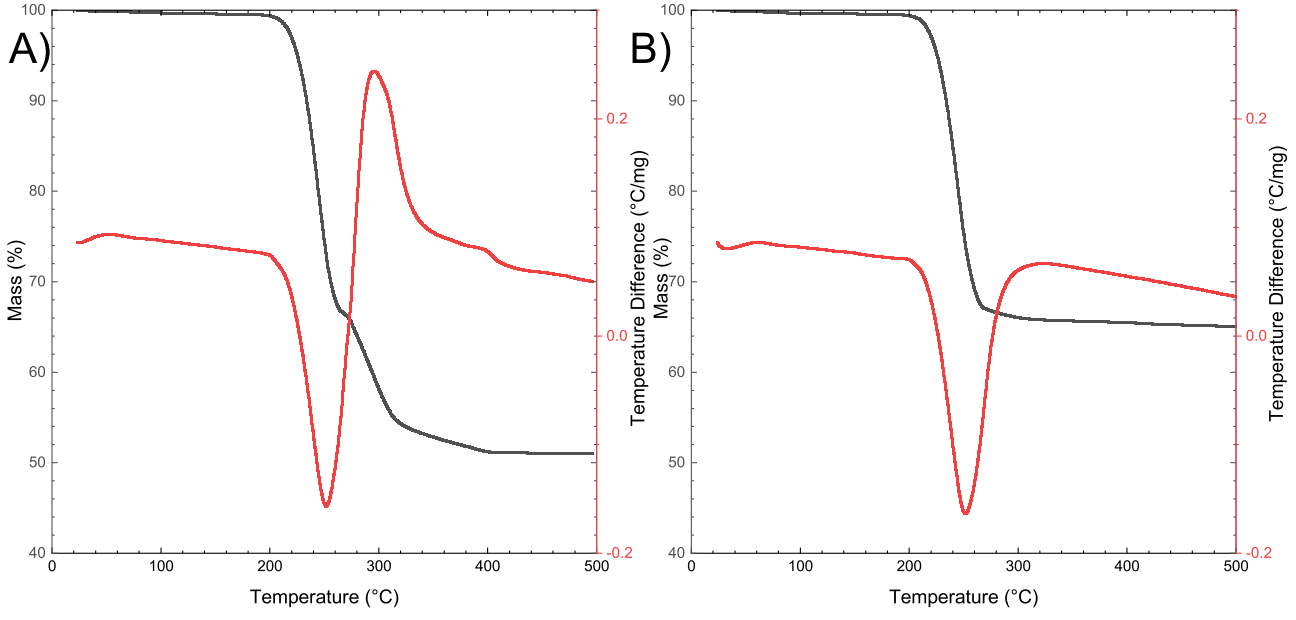

Fig. 3. DTA analysis: A) copper carbonate in the atmosphere of 95%Ar and 5% H_2, B) copper carbonate in the atmosphere of 100% Ar. Experimental conditions: gas flow 100 mL/min.

Table 2
The influence of temperature on the reaction rate.

T, °C	k_1	R^2	k_2	R^2
200	0.873 ± 0.0018	0.984	0.496 ± 2.38 × 10^{-4}	0.995
210	1.780 ± 0.03146	0.988	0.704 ± 0.00109	0.997
220	1.772 ± 0.01103	0.978	0.824 ± 0.00141	0.997
240	1.767 ± 0.0032	0.997	1.149 ± 0.00143	0.998

in the case of the second reaction, there is a clear influence of temperature on the speed of this process.

The activation energy of the reaction can be determined using logarithmic forms of the Arrhenius equation (Eq. (12)) (See Fig. 5)

$$lnk_x = lnA_x - \frac{E_{a,x}}{R \cdot T} \quad (12)$$

where:A_x – is the pre-exponential factor, min^{-1},R – gas constant.E_a – activation energy.

In the case of k_2, the linear correlation was found in the full range of studied temperatures. The activation energy was found to be equal to 40.73 $\frac{kJ}{mol}$, and the pre-exponential factor 1.66 · $10^4 min^{-1}$.

3.3. Influence of grinder time of copper(II) carbonate on the final copper powder size and size distribution

It is well known that copper particles' size (powder) can be changed by the grinding process. As mentioned in the introduction section, the process of grinding metallic copper is very energy-consuming. The cost of producing copper powders by this method is high, and the quality of the products obtained is moderate. This is due to the high plasticity of copper. The grinding process is also exothermic, which leads to stress relief from the particles. The accumulation of stresses leads to the cracking of the copper particles. So, we have two competing processes. As a result, the energy cost is high. In the case of copper(II) carbonate grinding, a significantly different case can be considered. First of all, this salt is easily grindable. The heat released by friction is consumed in the process of decomposing copper(II) carbonate into copper(II) oxide. Therefore, a series of tests were carried out in the work, where the milling times of copper carbonate were changed in the range from 10 to 180 s. We expected that this time should be sufficient to significantly grind the copper (II) carbonate. Obtained results are shown in Fig. 6.

As can be seen, an unexpected trend is observed. The grinding time did not reduce the mean value of the particle size. In fact, larger particles are observed after longer grinding times. For example, after 90 s of grinding time, particles with a diameter of 128 μm are observed. This phenomenon effectively limits the grinding process as a method of reducing the particle size of salt. To explain this problem, SEM analyzes of the selected samples were carried out. Obtained results are shown in Fig. 7 and Fig. 8.)

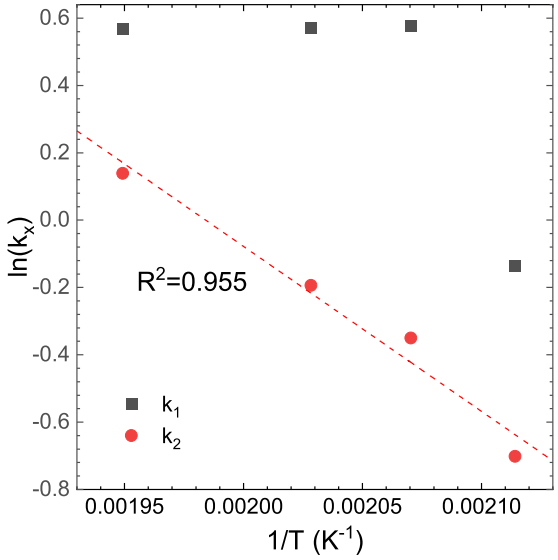

Fig. 5. Determination of activation Energy using Arrhenius dependence.

There is a significant difference in the obtained results between the SEM method and laser light scattering. It is probably related to the very strong electrostatic interactions of copper (II) salt particles and their aggregation. This electrostatic interaction is so strong that the analyzer (Malvern Mastersizer 2000) is not able to identify particles as separated ones. The existence of aggregates explains very well why longer grinding times result in apparently larger particles. It is clearly visible that the particles after the grinding process are much smaller. Therefore, in the further parts of the work, the histograms presented are based on the analysis of microscopic images.

Then, the ground salts were subjected to a reduction process with a hydrogen/argon mixture. All experiments were performed under identical conditions to check whether a grinding time in the range of 10–180 s had an effect on the size of the copper powders.

Scanning microscopy makes it possible to examine the morphology of the obtained powders. This method is reliable, provided that a sufficiently large statistical sample is made. In our case, we assumed that every time the measurement should be made for at least 100 particles at different fragments of the samples. In this way, the human factor and the pseudo-randomness of observations are eliminated.

SEM images were used to determine the particle size distribution. The results obtained are presented below (see Fig. 9).

In order to make it easier to interpret the obtained results, in Fig. 10, we present the average size and distribution of the average size of copper powders as a function of grinding time.

As expected, there is an influence of the grinding time on the size of the copper powders. It is surprising that the grinding time practically does not change the size distribution. The change is significantly noticeable after 10 and 30 s. This is, of course, related to the type of grinder used. The centrifugal force causes the particles to quickly settle on the walls of the grinder, as a result of which longer grinding is ineffective.

3.4. The influence of temperature on the copper powder size and size distribution

As shown by the fallout results in Chapter 3.2 Process rate studies, one of the important parameters of the process of obtaining copper powders is the temperature of the process itself. The results obtained from SEM images are presented (see Fig. 9 and Fig. 11).

In order to make it easier to interpret the obtained results, in Fig. 12, we present the average size and distribution of the average size of copper powders as a function of the temperature of the process.

Using a higher temperature speeds up the process. It can also lead to local overheating of the material and, as a result, sintering and grain aggregation.

3.5. XRD analysis

The XRD pattern of the fine Cu powder obtained is shown in Fig. 13. No extra diffraction peaks corresponding to CuO, Cu_2O, or $CuCO_3$ phases are detected, indicating that pure Cu fine powder was successfully produced. The intensity of the peaks is sharp and narrow, confirming that the sample is of high quality with good crystallinity and fine grain size.

From XRD results and using Williamson-Hall's method, the crystalline size was calculated. This theory states, that the broadening of the peak comes from a strain of the lattice and crystalline size (Eq. (13))

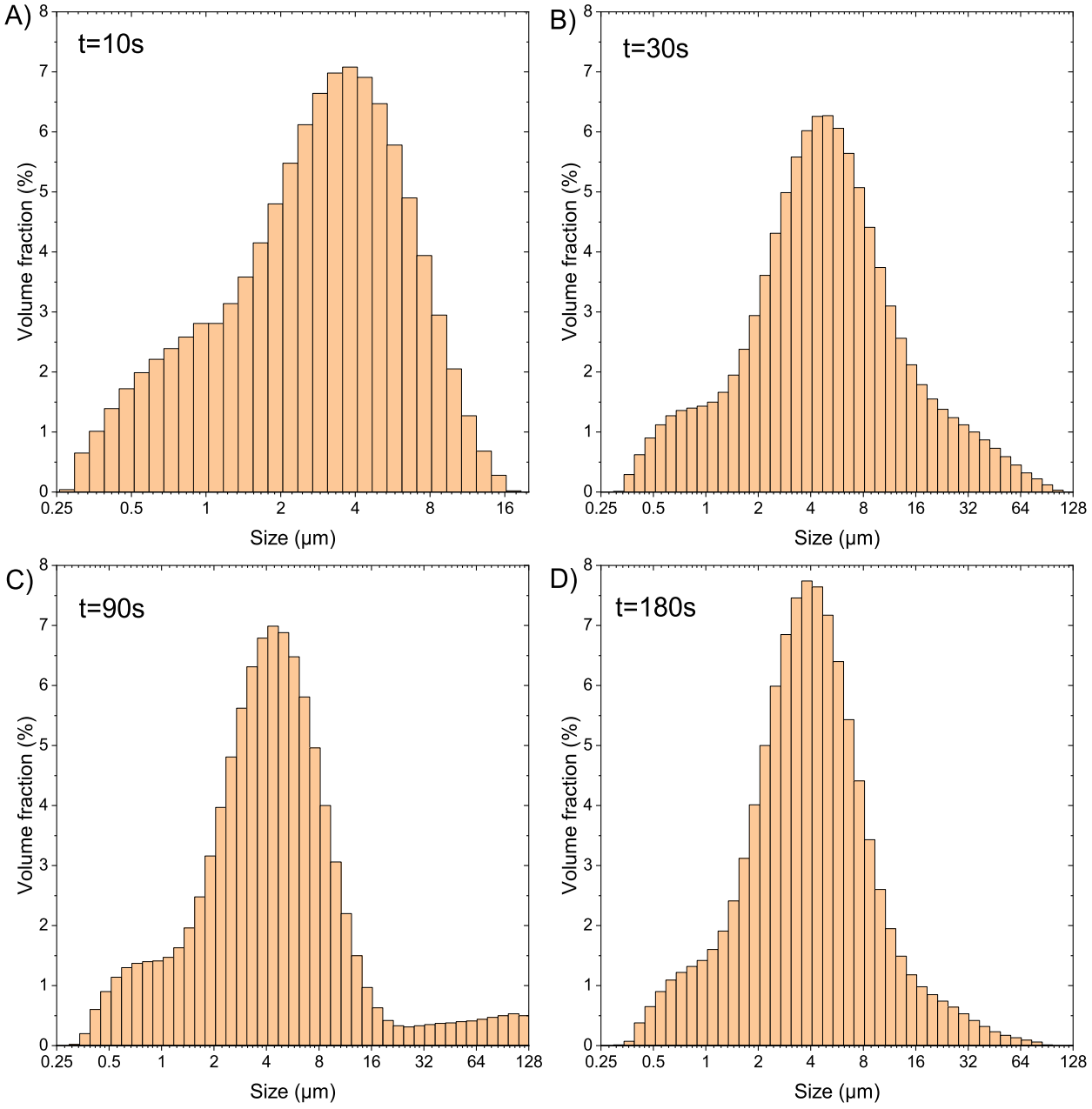

Fig. 6. The influence of grinding time of copper(II) carbonate on the final size of particles.

$$\beta_T = \beta_D + \beta_\varepsilon \tag{13}$$

where β_T is broadening of the peak, β_D is broadening from the crystalline size, and $\beta\varepsilon$ is broadening caused by strain. By transforming Sherrer's equation (Eq. (14)) we know that:

$$\beta_D = \frac{K\,\lambda}{D cos\theta} \tag{14}$$

The Broadening caused by microstrain is given by (Eq. (15)):

$$\beta_\varepsilon = 4\,\varepsilon tan\theta \tag{15}$$

By putting Eqs. (14) and (15) into Eq. (13) and after multiplying both sides by cos(θ) The following equation was obtained:

$$\beta_T cos\theta = \varepsilon(4sin\theta) + \frac{K\,\lambda}{D} \tag{16}$$

By comparing it (Eq. (16)) to the standard line equation we can determine the size component by calculating the intercept value (.

Fig. 14). The final equation needed to calculate the crystallite size by Willamson-Hall's method is shown in Eq. (17).

$$D_{W-H} = \frac{K\,\lambda}{C} \tag{17}$$

According to the obtained result, the size of the produced copper crystallites is equal to 63.6 nm. Small grain size has a negative impact on the conductivity of the material due to many grain boundaries since they reduce the free flow of electric charge but also are responsible for stronger mechanical properties of obtained products from this material.

3.6. BET analysis

We conducted BET analyzes to verify the degree of surface devel-

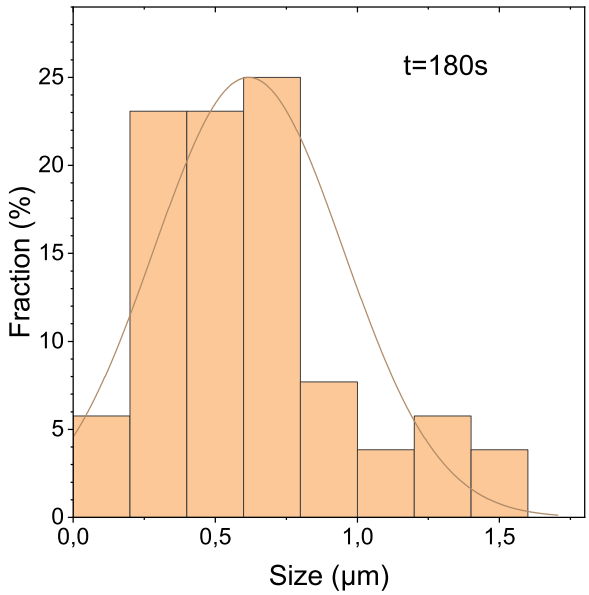

Fig. 7. Copper(II) carbonate particle size distribution determined using SEM image. Experimental conditions: grinding time 180 s. The number of particles analyzed was $n = 52$.

opment. It should be expected that as a result of the reaction, the Cu (II) ions will be reduced to Cu (0). This is accompanied by a change in the density of the material. The density of solid copper is $8.96\frac{g}{cm^3}$, and copper carbonate is $4.0\frac{g}{cm^3}$. We expect the resulting copper powder to be porous at low temperatures. The diffusion of atoms on the surface is very slow, making it impossible to minimize surface energy and obtain spherical solid particles. The results obtained using the BET method as well as calculated from DLS measurements (Mastersizer) are shown in Table 3.

The algorithm used by the Mastersizer device calculates the surface area of the particles taking into account their hydrodynamic radius. This method is not sensitive to the porosity of the material. As can be observed in Table 3, there is a correlation between results obtained from BET and DLS. As the process temperature increases, the surface of the powder is less developed. The influence of the grinding time of copper (II) carbonate on the particle size was also investigated. The results obtained are presented in Table 4.

There is apparently a decrease in surface area due to grinding. The conducted ANOVA test, whether there is a linear correlation between the grinding time and the surface area, clearly indicates that there is no such correlation. So basing only and solely on BET measurements may also be inappropriate.

3.7. XRF study

The results of the chemical composition measurements are presented in Table 5. Due to the signal from silicon observed in each sample (most likely resulting from the SiO_2 sample holder), the results of the analysis were calculated disregarding the silicon content. The composition for both calculation variants was reported. Additionally, the values of matching the measured spectrum to the theoretical spectrum (R / R0) were given, confirming the correctness of the performed measurements. The measured sample was powder reduced at a temperature of 300 °C.

Even for the lowest of tested temperatures, the obtained powder shows high purity. This result backed further by the results from XRD analysis confirmed that the reaction has been entirely completed.

3.8. Conductivity test of obtained powders

The conductivity test was based on the measurements presented by Juan et al. [65]. The measuring system consisted of a cylindrical die of

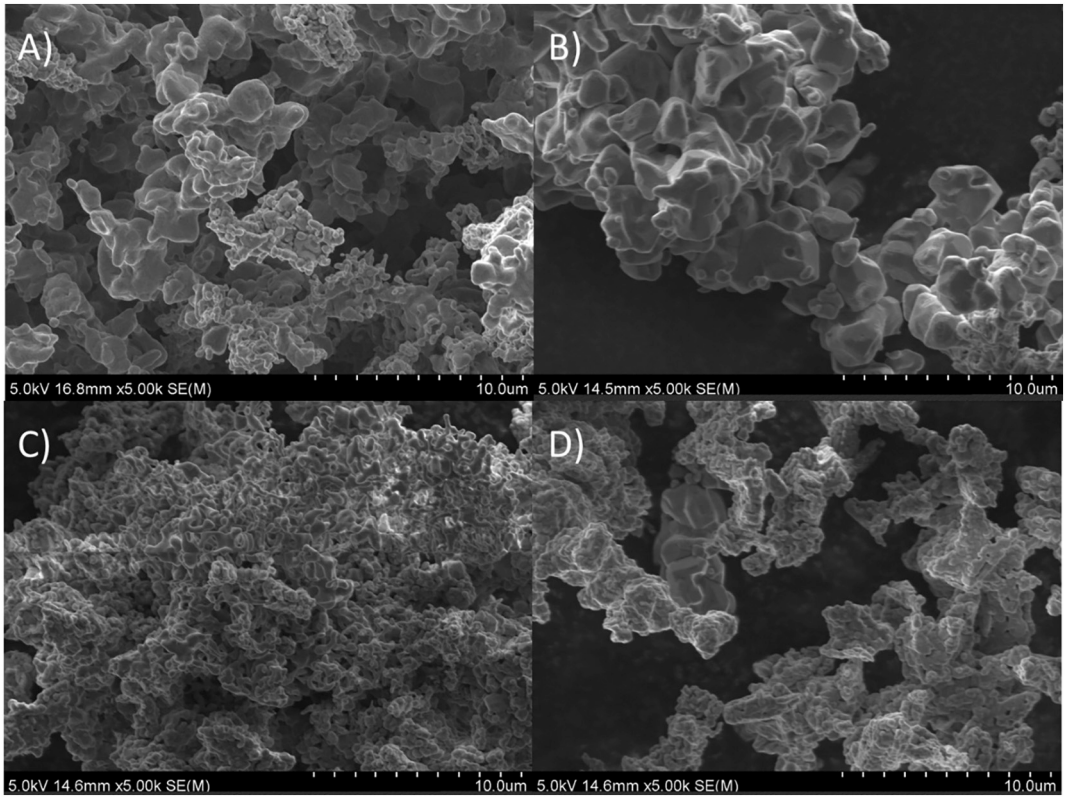

Fig. 8. SEM image of copper powder synthesized at 300 °C, synthesized from carbonate ground for different times. A)10 s, B)30 s, C)90 s, and D)180 s.

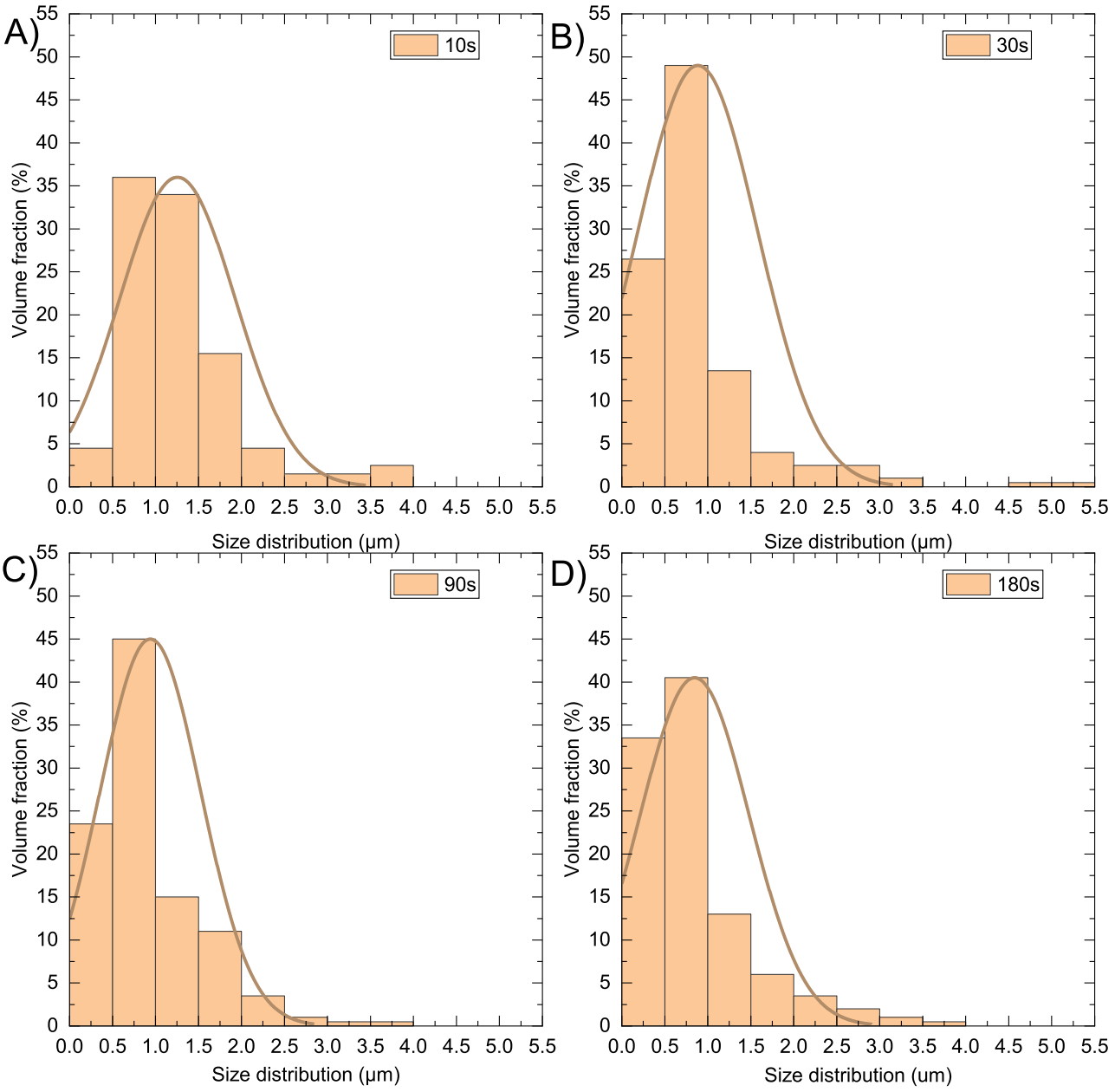

Fig. 9. The influence of grinding time of copper(II) carbonate on the final size of copper powder. Experimental conditions: $T = 300$ °C, gas flow rate 20 L/h, time: of reduction 2 h, heating rate 5 °C/min.

an electrically insulating material (Teflon, $\sim 10^{12}$ Ω m), two brass pistons, and two copper sheets covert with insulating sheets from one side. The test procedure was as follows: a known amount of powder was poured into the Teflon die and stoppered by the bottom piston. Next, the setup was shaken and the rest of the powder fit into the die. After that, the top piston was mounted and the assembly was put into the hydraulic press, isolated from it by two copper sheets covert from one side with insulating sheets. After that, the copper sheets were connected to the Ohmmeter and the resistivity and distance between the ends of the pistons has been measured. By measuring that distance, it was possible to calculate the volume occupied by copper powder and further compaction degree. The powder mass porosity was reduced by increasing the load along the upper piston. Resistance measurements were carried out for all porosities at room temperature (approx. 25 °C). The scheme of the experimental assembly is presented in Fig. 15.

As can be seen in Fig. 16, for low compaction degree values, there is almost no visible increase in conductivity. It is caused by an extremely high resistance starting value (40 MΩ). The obtained conductivity values are consistent with the literature [66]. The conductivity of copper is equal to 5.79×10^7 S/m. Even after taking into consideration that powder material, no matter the compaction degree will never reach the conductivity of bulk material the obtained values of the copper powder are very underwhelming. The reason behind this is nanometric scale crystallites size. The grain boundaries are barriers to electron flow, which is why the metal with less structure deformation and larger grain size will have much higher conductivity.

The nano-size grains are also the reason why the obtained powder is strongly reactive with air, which results in rapid oxidation of the powder. Even if the XRD analysis shows no proof of CuO and Cu_2O phases, we cannot dismiss the possibility of extremely thin oxide film on the surface of the powder. The conductivity of copper is extremely dependent on the purity of the material which is why even a small amount of

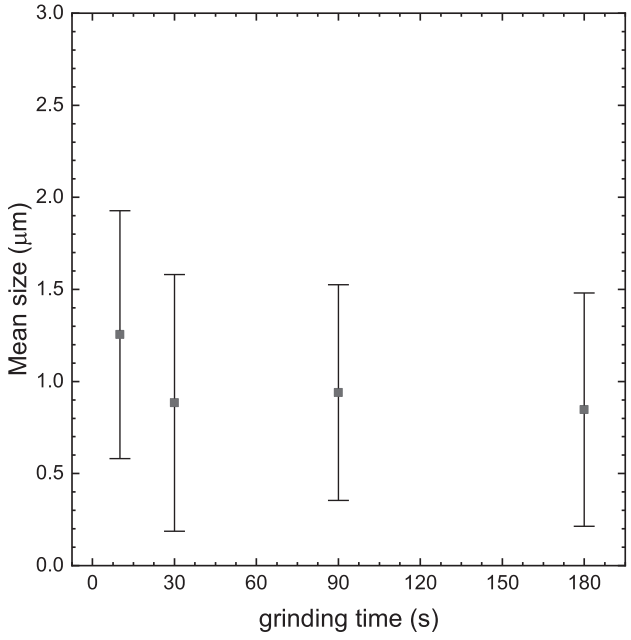

Fig. 10. Statistic analysis of the influence of grinding time on mean size and size distribution.

the oxide, especially at the interface between particles can cause a significant decrease in the conductivity.

The obtained powder was produced with conductive paste production in mind. At later stages of this process, copper powder is sintered. That is why initially low conductivity of the pure powder does not limit its application in conductive pastes and good compatibility caused by the small particle size and round-like shape of the particles are more important.

The obtained copper powders, after synthesis, must be stored in an inert gas atmosphere. They undergo quick oxidation due to low particle size. While maintaining the protective atmosphere, no influence of the storage time on the properties of the powder is observed. At work, the powders were stored in a mixture of Ar + H_2 (95: 5%). Conductivity measurements were made on powders, 3 months after their synthesis.

3.9. Sustainable metrics

As with other heavy metal derivatives production, copper powder synthesis raises an environmental challenge. Overall, copper production annually demands about 600 million GJ of energy contributing 0.21% greenhouse gas emission among all-metal production [67]. This is even more evident when assessing the environmental impact along with the Green Chemistry principles such as the process mass index (PMI), which would show an unfavorable ratio of process mass inflow as rated by the product outflow. Accordingly, fresh ideas on process design, as proposed in this paper, may attenuate the environmental footprint, and recycling and circular-flowing processes are effective in reducing the PMI. Those ideas follow the "R framework" of sustainability science [68], and among those principles three *"R's"* are applied in this work, which are reduce, reuse and recycling. It has to be, however, noted that recycling loops involve secondary processes, which might generate additional secondary waste and/or impacts. In this perspective, a life cycle assessment (LCA) of the process proposed here is conducted [69], which is benchmarked with current copper processes on atomization, electrolysis, hydrometallurgy, or solid-state reduction. Regarding bulk copper production, LCA studies have been described for diverse methodologies regarding pyrometallurgical and hydrometallurgical productions [70–72]. Besides that, Song et al. [73] and Kulczycka et al. [74] quantified the environmental impact of copper processes and, based on this, proposed alternatives for reducing energy use and environmental impact.

The LCA of the process proposed here investigates both the first, following and last cycles since recycling loops are initialized after the first cycle, see Fig. 1. Analogously, the last cycle stops with recycling. The following assumptions on the material's conversion were taken: >98% of carbon dioxide is adsorbed, trapped as carbonate, and stored as such. Chlorine gas is bound to the metallic copper bulk, trapped as copper chloride, and stored as such. Hydrogen and argon gases are considered as waste, despite hydrogen might be burned before being emitted or transferred to another use as a chemical or fuel.

The sustainability assessment is performed in a cradle-to-gate fashion using 1 kmol of the copper powder as a functional unit. The study was performed using GaBi LCA modeling software provided with database 2020 and using the Ecoinvent impacts database. Recipe 2016 v.1.1. was taken as quantification criteria. Taking the no-waste generation policy, the model assumed stoichiometric equivalence of reagents. Copper (II) nitrate was separated considering bulk copper, Cu (bulk), and nitric acid as raw materials. Energy sources were taken in the most unfavorable conditions considering EU-28 average sources.

Based on the procedure described above, Table 6 shows the inventory of the starting and the other cycles. Once the recycling is initiated after the first cycle, the successive cycles include only bulk copper and energy as inputs.

LCA results of environmental impacts of the first cycle are shown in Table 7. This step is chosen because it is the most unfavorable due to the larger amount of raw materials needed for starting the main process, including recycling. Not surprisingly, all impact categories are high. Among those, the highest scores are given for the global warming potential (GWP) with 879 kg CO_2-eq./kmol, fossil depletion with 238 kg oil eq/kmol, and terrestrial ecotoxicity with 23,197 kg 1,4-dB eq./kmol. Other relevant impacts are found for freshwater consumption with 6.28 m^3/kmol, freshwater ecotoxicity with 0.911 kg 1,4-dB eq/kmol, and marine ecotoxicity at 11.6 kg 1,4-dB eq/kmol. Taking a pyrometallurgical Cu *(bulk)* process for a rough comparison, the process by Dong et al. [67] reported a GWP of 315 kg CO_2-eq/kmol, an abiotic depletion-elements of 43 kg Sb-eq/kmol, a freshwater ecotoxicity of 7067 kg 1,4-DCB-eq/kmol, and photochemical oxidation of 0.701 kg ethylene-eq/kmol. Additionally, the same reference described the impacts regarding a hydrometallurgical method for Cu *(bulk)* production, scoring a GWP of 395 kg CO_2-eq/kmol, an abiotic depletion-elements of 34 kg Sb-eq/kmol, a freshwater ecotoxicity of 23,718 kg 1,4-DCB-eq/kmol, and photochemical oxidation of 0.158 kg ethylene-eq/kmol. Those literature-reported values are lower than the values obtained in the first cycle of the proposed process in this paper, but in the same impact range concerning the successive cycles once when recycling is effective. It has to be acknowledged that, while the literature values refer to the production of bulk copper, our process described produces a high-quality copper product at the same environmental expense; thus sustainability impact per product value is higher for our process.

The share of impacts stemming from the ecological backpack from Ar and Cu inputs into the LCA scores is evident when compared to the case of the first cycle scenario when those impacts are considered to be absent. Fig. 17(left) shows that this leads to a decrease of about 40% or higher in 8 over 18 categories, considered in this study. Especially relevant are the stratospheric ozone depletion and marine eutrophication with a reduction of around 80% and 60%, respectively. The GWP is reduced by half when not considering Ar and Cu in the first cycle scenario. These results are in accordance with the literature since Cu has significant ecotoxicity and human health risks, as reported by Chen et al. [75] regarding mobile phone wastes, ranging from 52,344 to 123,937 PAF·m^3·day·kg^{-1}. The score for Cu is the most significant of all heavy metals considered in this analysis. In this case, the influence of Cu-containing material on the overall environmental impact is about 58%. Similar results are also obtained regarding the utilization of waste

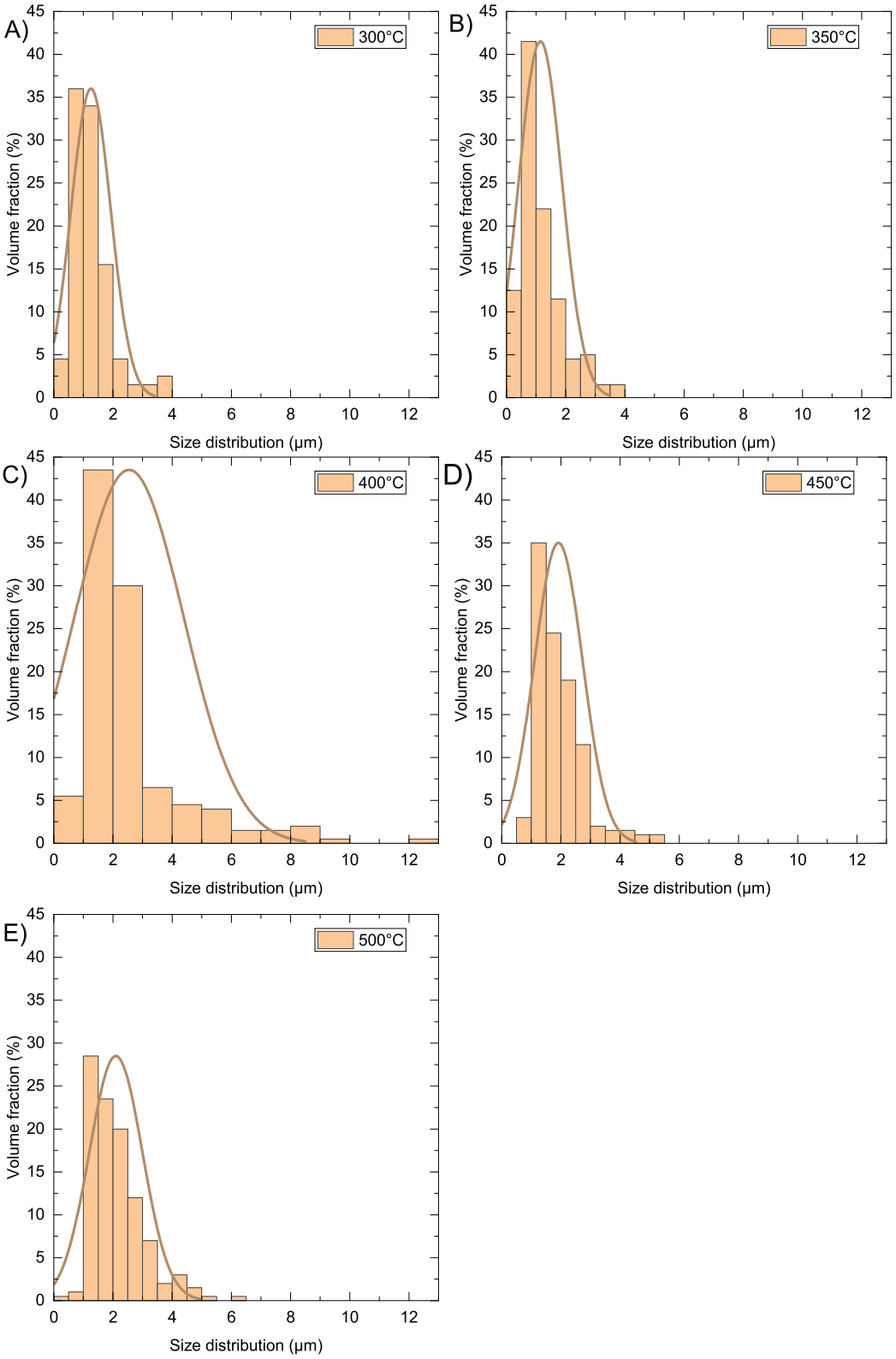

Fig. 11. The influence of temperature of reduction on the particle size and size distribution.

printed circuit boards, where the Cu impact is highest in a range of 13,273–28,153 PAF·m^3·day·kg^{-1}. [76] In the latter case, the Cu share on environmental impact is almost 90%.

In our process, once the first cycle is completed, the environmental footprint turns much more favorable. Due to recycling, no loading of materials is necessary anymore. As shown in Fig. 17(right), most of the LCA impacts show about a 60% decrease for the second and successive cycles as compared to the first one, and some even have significant reductions approaching 95%. Only the metal depletion impact keeps high (10% increase over the first cycle) because of the Cu *(bulk)* reload.

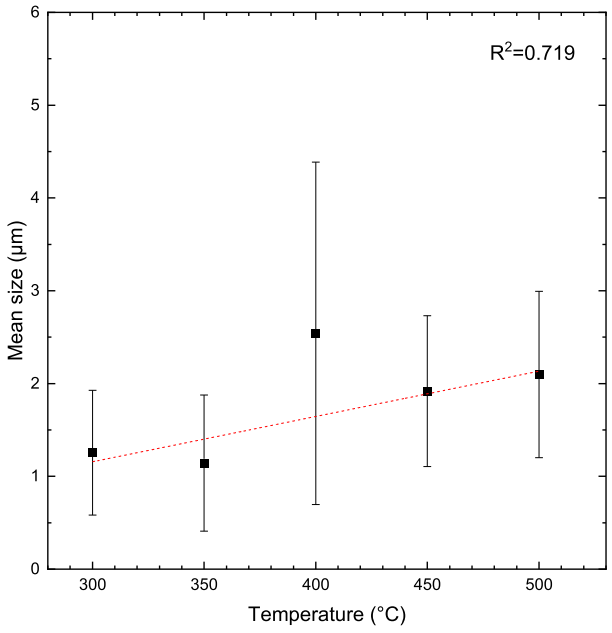

Fig. 12. Statistic analysis of the influence of temperature of the process on mean size and size distribution.

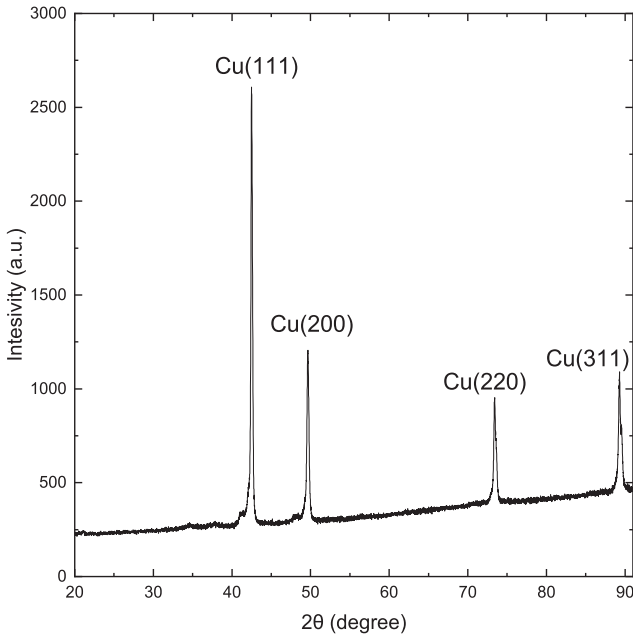

Fig. 13. X-ray diffraction pattern of Cu fine powder obtained in reduction process with the temperature of 300 °C.

Since the proposed recycling processes lead to a relevant reduction of environmental impacts, an extended production time could almost vanish the negative impact of the first cycle. Recycling should also affect the circularity of the process. Assuming that both Ar and H_2 would be wasted in the last cycle, a recycling factor (F_R) of 0.87 can be calculated. Nevertheless, the recycling efficiency (E_F) is highly influenced by the waste generation of the last cycle, which delivers a lower value of 0.4. These parameters sum up to a material circularity indicator (*MCI*) for the whole process of 0.56 if the first production cycle is considered. MCI is the main circularity index that indicates the degree of restorative

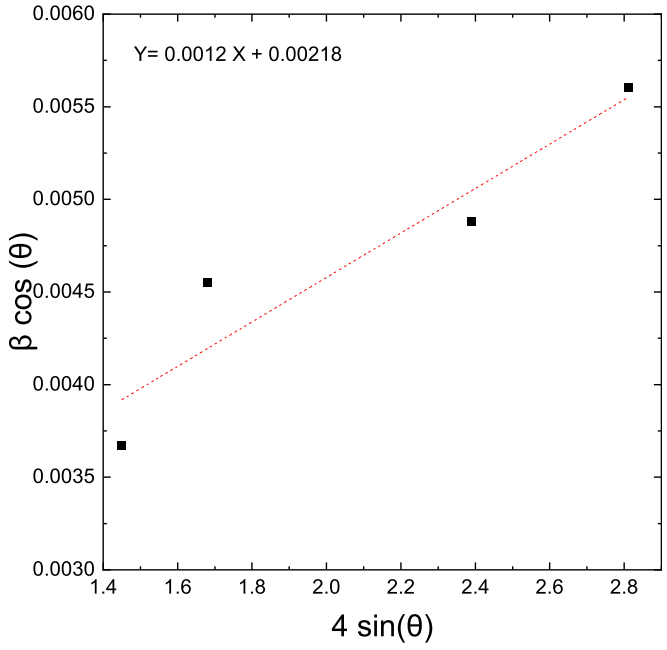

Fig. 14. Plot of $\beta\cos(\theta)$ vs $4\sin(\theta)$ of Cu fine powder sample.

Table 3
Analysis of the structure of the material.

The temperature of synthesis, °C	Surface area (BET), m^2/g	Specific Surface Area (DLS), m^2/g
300	1.410 ± 0.004	0.220
350	1.125 ± 0.002	0.214
400	0.952 ± 0.007	0.125
450	0.650 ± 0.007	0.084
500	0.554 ± 0.005	0.091

Table 4
Size of $CuCO_3$ particles used for Cu powder synthesis.

Grinding time, s	Surface area (BET), m^2/g	Specific Surface Area, m^2/g – obtained from Mastersizer
10	2.727 ± 0.009	3.33
30	2.671 ± 0.009	2.31
90	2.049 ± 0.008	2.35
180	2.049 ± 0.008	2.41

Table 5
The chemical composition of Cu fine powder obtained in the reduction process with the temperature of 300 °C, obtained from the XRF method.

Sample name	Amount (%)					R/R_0
	Cu	Si	P	Cl	Ca	
Cu powder red. 300 °C	94.91	4.74	0.11	0.05	0.19	4.8
	99.65	–	0.11	0.05	0.19	4.5

material flows. This indicator can be higher by allowing the production in consecutive cycles since e.g. the waste generated in the last cycle would remain in the same order of magnitude, while the Cu powder production would increase.

Finally, the energy consumption of conventional methodologies based on electrolytic and atomization pathways to produce Cu powder shall be compared to the approach proposed in this paper. Using the conventional electrolytic route, the power consumption per ton of final product is given as 3800–4200 $kWh.t^{-1}$, while the atomization route

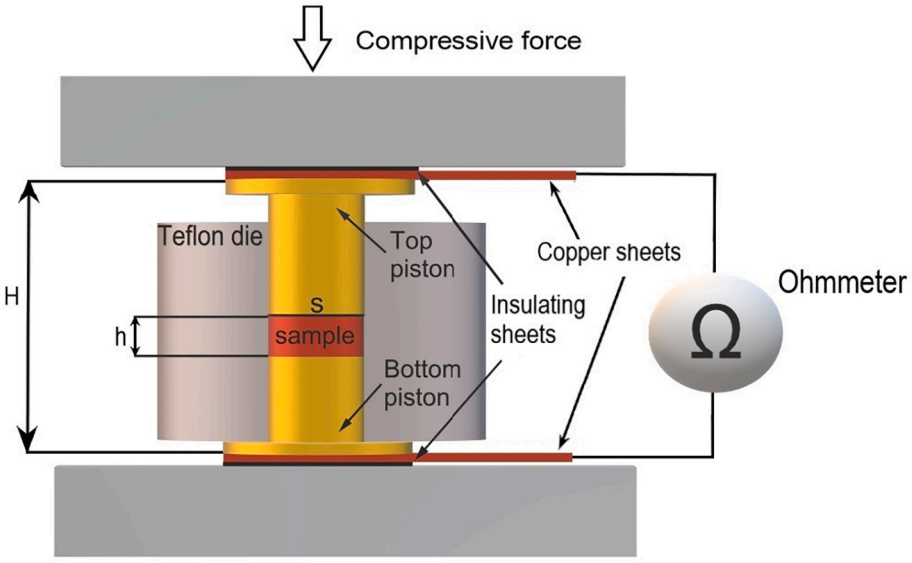

Fig. 15. Scheme of experimental measuring assembly.

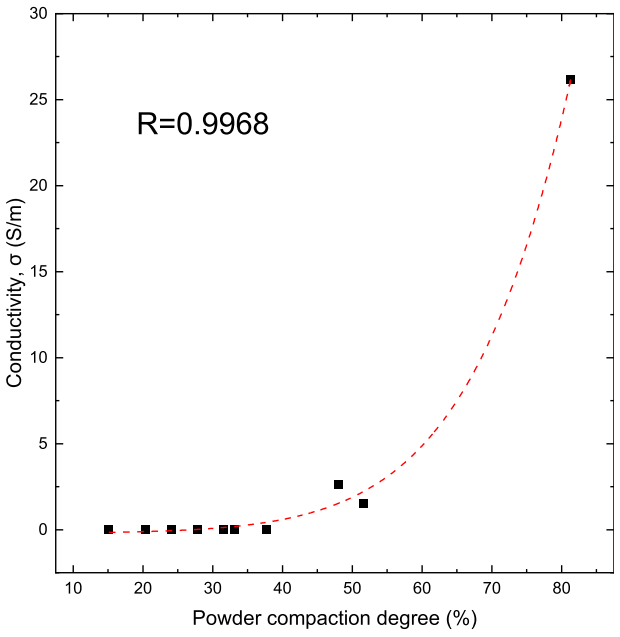

Fig. 16. Conductivity of pressed powder in the function of compaction degree.

takes around 2000 kWh.t^{-1} [2]. The process described in this paper needs 5000 kWh.t^{-1}, thus being higher than for the conventional processes but still within the same order of magnitude. While Xia et al. [36] report a low power consumption for the electrolytic route as 719 kWh.t^{-1} the particle size of the product is almost 50 times larger. Thus, to produce the powders with similar properties the power consumption would be significantly larger and it is incomparable to the method proposed in this paper. The heat transfer from Ar to $CuCO_3$ recycled in the main reaction with an efficiency of 85% has a major effect on the overall energy efficiency. Thus, the total environmental effect is two-fold: the higher energy need of the new proposed process is counterbalanced by its benefits in materials recycling and waste avoidance.

Table 6
Life Cycle Assessment inventory for each process stage for the production of 1 kmol copper powder.

First cycle inputs			Other cycle inputs	
Item	Sublevel	kg/ kmol Cu		
KCl		149.1	Cu (bulk)	63.54 kg/ kmol Cu
Ar + H_2			Energy	230 kWh/ kmol Cu
(95:5)	Ar	760		
	H_2	2		
$CuCO_3$				
	$Cu(NO_3)_2$	187.56		
	Na_2CO_3	106		
	Water	99		
KOH		112.2		
H_2O		36		
H_2O		36		
Energy	230 kWh/ kmol Cu			

Table 7
Environmental impacts obtained in the first and successive cycles of copper powder production.

Sustainable impacts	Process step	
	First cycle	Successive cycles
Climate change, incl biogenic carbon [kg CO2 eq.]	879	325
Fine Particulate Matter Formation [kg PM2.5 eq.]	0.624	0.123
Fossil depletion [kg oil eq.]	238	101
Freshwater Consumption [40]	6.28	1.36
Freshwater ecotoxicity [kg 1,4 dB eq.]	0.911	0.0183
Freshwater Eutrophication [kg P eq.]	0.00217	0.000813
Human toxicity, cancer [kg 1,4-dB eq.]	0.43	0.0742
Human toxicity, non-cancer [kg 1,4-dB eq.]	365	6.22
Ionizing Radiation [kBq Co-60 eq. to air]	7.82	2.19
Land use [Annual crop eq.·y]	423	10.8
Marine ecotoxicity [kg 1,4-dB eq.]	11.6	0.0527
Marine Eutrophication [kg N eq.]	0.0294	0.0186
Metal depletion [kg Cu eq.]	115	127
Photochemical Ozone Formation, Ecosystems [kg NOx eq.]	1.42	0.613
Photochemical Ozone Formation, Human Health [kg NOx eq.]	1.407	0.608
Stratospheric Ozone Depletion [kg CFC-11 eq.]	0.00146	0.00113
Terrestrial Acidification [kg SO2 eq.]	1.896	0.346
Terrestrial ecotoxicity [kg 1,4-dB eq.]	23,197.4	54.6

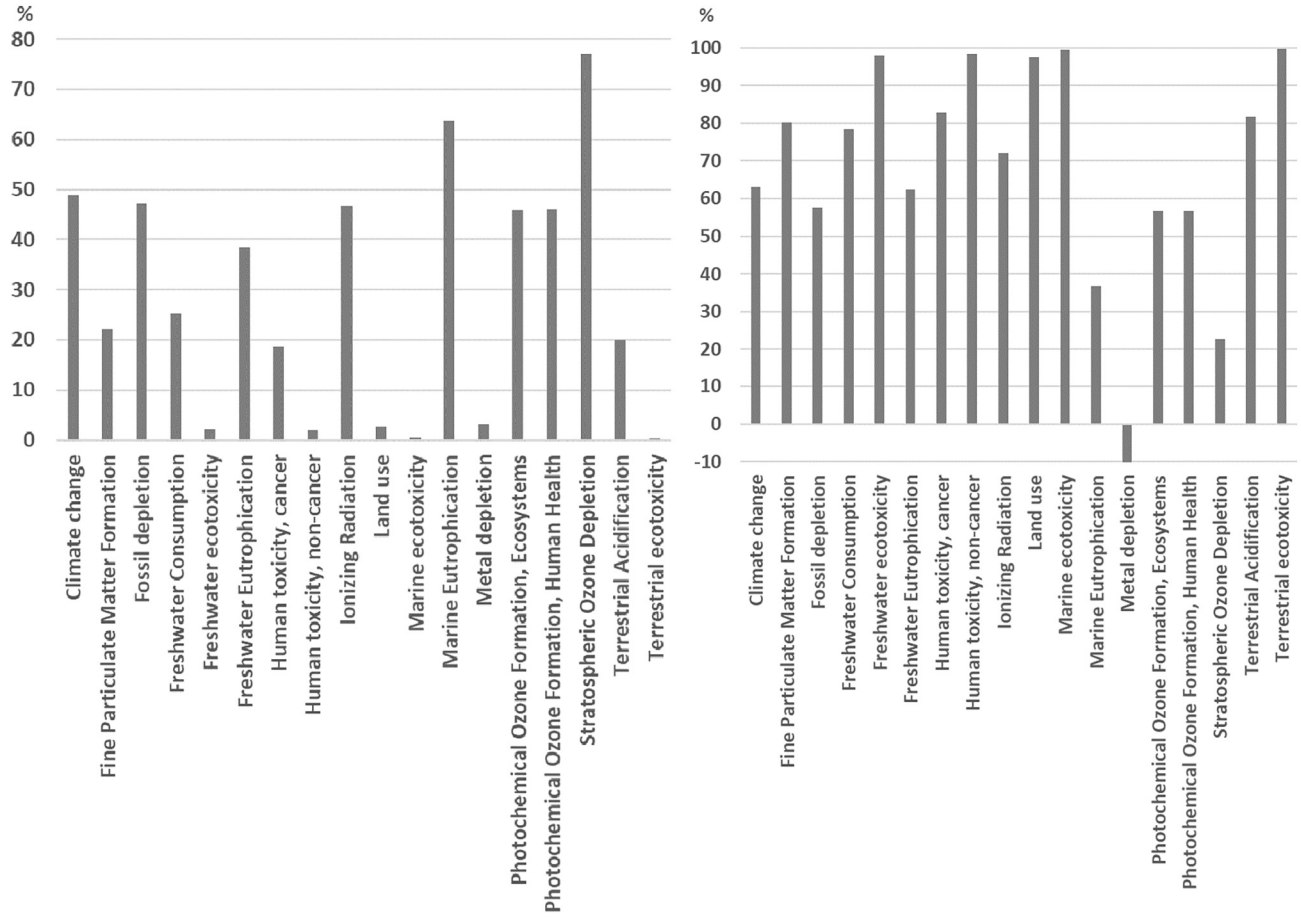

Fig. 17. Percentage of impacts reduction in the first cycle scenario when Cu (bulk) and Ar impacts are not considered, (left) and percentage of impacts reduction when the second cycle is compared with the first one (right).

4. Conclusion

The paper proposes a technology for producing copper powders using a thermochemical wasteless method. The proposed technology is based on known electrochemical, chemical, and thermal reactions. Each step has been analyzed with a comparison to existing scientific literature showing the practical applicability at every stage. The influence of parameters such as the reduction temperature of copper carbonate and the grinding time of copper carbonate on the size and size distribution of the obtained powders was investigated in detail. The performed research showed that these factors affect the size and size distribution of the copper powder. XRD study shows no extra diffraction peaks corresponding to CuO, Cu_2O, or $CuCO_3$ phases are detected, indicating that the pure Cu fine powder was successfully produced. The XRF analysis further proves the high purity of the obtained product. The crystallite size calculated from Williamson-Hall's method was equal to 63.6 nm. The nanometric scale crystallites cause high reactivity of obtained powder with air and rapid oxidation of copper. Due to this problem, the produced fine copper powder needs to be stored in an inert gas atmosphere. Although the results from the conductivity test of produced powders showed low conductivity, the melting stage in the conductive paste production process eliminates this problem. Therefore, the results suggest the potential applicability of the studied method for the mass production of high-quality copper powders with zero environmental impact. While the first cycle energy consumption is equal to 230 kWh/kmol Cu, in the subsequent cycles only power is needed to be supplied, where other substrates are circulating as shown in the provided technology concept. Even though the energy needed to produce this powder is high, the neutral-to-environment technology, high purity, and mean grain size as low as 1 μm, show the great potential of this technology. An LCA assessment of the process shows improvements for several major LCA impact categories due to the recycling of the chemicals involved in the process. The first and last cycles are different from the many production cycles which they encompass and which exert the recycling. The latter shapes the environmental profile and shows that the process idea presented in this paper is sustainable. This is also expressed when bringing these effects into a single value, which is the mass circularity indicator (MCI), scoring 0.56. Most of the LCA impacts show significant decrease percentages when comparing the second and successive cycles scenario with the first cycle one, ranging between 60 and 90% decrease in most cases. The new process profits from a long run cycles, meaning a high number of production cycles, since then relatively lower waste is created, relative to that made in the first cycle.

Credit author statement

Filip Cebula – Investigation
Konrad Wojtaszek – Investigation
Hasan Shabbir – Investigation
Anna Kula – Investigation
Zbigniew Pędzich – Investigation
Kamil Kornaus – Investigation
Stanisław Małecki – Investigation
Karolina Kołczyk-Siedlecka – Investigation
Robert P. Socha – Investigation, conceptualization
Marc Escribà-Gelonch - Writing - Original Draft, Formal analysis.
Katarzyna Rogóż - Conceptualization.
Michael Goodsite - Writing- Reviewing and Editing.

Volker Hessel - Writing- Reviewing and Editing.
Marek Wojnicki - Writing- Original draft, Supervision.

Declaration of Competing Interest

The authors declare no conflict/competing of interest.

Acknowledgment

This work was supported by project from Intelligent Development Operational Program 2014–2020, co-financed by the European Regional Development Fund, project No. POIR.01.01.01-00-1246/20-00.

References

[1] O.D. Neikov, S.S. Naboychenko, N.A. Yefimov, Editors., Technologies and Applications, in Handbook of Non-Ferrous Metal Powders, Second edition, Elsevier, Oxford, 2019, p. iv.
[2] S.Z. Jingguo Zhang, Limin Wang, Jinghuai Zhang, Ligen Wang, Jian Zhang, He Dai, Copper and copper alloy powder technology and market developments in China, Powder Metall. 57 (5) (2014) 314–315.
[3] V.K. Mohan, M. Shamnadh, A. Sudheer, Fabrication and characterization of friction stir welding of AA6061 using copper powder, Mater. Today Proc. 5 (11) (2018) 24339–24346, https://doi.org/10.1016/j.matpr.2018.10.229.
[4] C.S. Abima, et al., Microstructural, mechanical and corrosion properties of aluminium MIG welds reinforced with copper powder, Int. J. Adv. Manuf. Technol. 105 (12) (2019) 5181–5190, https://doi.org/10.1007/s00170-019-04546-9.
[5] L. Ledoux, C. Prioul, Fatigue and fracture of porous steels and Cu-infiltrated porous steels, in: Pm2Tec'98, International Conference on Powder Metallurgy & Particulate Materials, Las Vegas, Nevada, USA, 1998.
[6] P. Lowhaphandu, J.J. Lewandowski, Fatigue and fracture of porous steels and Cu-infiltrated porous steels, Metallur. Mater. Trans. A 30 (2) (1999) 325–334, https://doi.org/10.1007/s11661-999-0321-4.
[7] S. Takaki, et al., Effect of copper on tensile properties and grain-refinement of steel and its relation to precipitation behavior 45 (7) (2004) 2239–2244.
[8] H.S. Tekce, D. Kumlutas, I.H. Tavman, Effect of particle shape on thermal conductivity of copper reinforced polymer composites, J. Reinf. Plast. Compos. 26 (1) (2007) 113–121, https://doi.org/10.1177/0731684407072522.
[9] K. Kassym, A. Perveen, Atomization processes of metal powders for 3D printing, Materials Today: Proceedings 26 (2020) 1727–1733, https://doi.org/10.1016/j.matpr.2020.02.364.
[10] Y.-L.X. Li-Tsung Sheng, Shu-San Hsiau, Chih-Peng Chen, Po-Shen Lin, Kuo-Kuang Jen, A study of pneumatic conveying with high-density AM-using metal powder in a pipe bend, Int. J. Mech. Sci. 181 (2020) 105763, https://doi.org/10.1016/j.ijmecsci.2020.105763.
[11] X.Z. Yuan-Hui Chueh, Jack Chun-Ren Ke, Qian Li, Chao Wei, Lin Li, Additive manufacturing of hybrid metal/polymer objects via multiple-material laser powder bed fusion, Additive Manufacturing 36 (2020), 101465, https://doi.org/10.1016/j.addma.2020.101465.
[12] N.A. Kirstin Riener, Stefan Ziegelmeier, Robert Ramakrishnan, Lukas Haferkamp, Adriaan B. Spierings, Gerhard J. Leichtfried, Influence of particle size distribution and morphology on the properties of the powder feedstock as well as of AlSi10Mg parts produced by laser powder bed fusion (LPBF), Additive Manufacturing 34 (2020), 101286, https://doi.org/10.1016/j.addma.2020.101286.
[13] Y.Z. Hongze Wang, Microscale interaction between laser and metal powder in powder-bed additive manufacturing: conduction mode versus keyhole mode, Int. J. Heat Mass Transf. 142 (2019), 118473, https://doi.org/10.1016/j.ijheatmasstransfer.2019.118473.
[14] G.A.F. Xuesong Gao, Wei Zhang, Kevin R. Wheeler, Numerical analysis of non-spherical particle effect on molten pool dynamics in laser-powder bed fusion additive manufacturing, Comput. Mater. Sci. 179 (2020), 109648, https://doi.org/10.1016/j.commatsci.2020.109648.
[15] M. Musztyfaga-Staszuk, et al., Copper-based volumetric filler dedicated for ag paste for depositing the front electrodes by printing on solar Si cells, Materials 11 (12) (2018), https://doi.org/10.3390/ma11122493.
[16] N. Prabaharan, M.A. Rosen, P.E. Campana, Recent Developments in Photovoltaic Materials and Devices, 2019.
[17] J.M. Gee, Cu paste Metallization for Silicon Solar Cells, 2011.
[18] G. Caveney, Silver is More 'Rich Man's Copper' Than 'Poor Man's Gold' [cited 2022 15.04.2022]; Available from: https://seekingalpha.com/article/4404413-silver-is-rich-mans-copper-poor-mans-gold, 2021.
[19] S.L. Brittany, et al., Photovoltaic (PV) Module Technologies: 2020 Benchmark Costs and Technology Evolution Framework Results, National Renewable Energy Laboratory, 2020.
[20] K. Gawlinska-Necek, et al., Silicon solar cells and modules with front contact paste containing copper-based component, Prog. Photovolt. Res. Appl. 29 (9) (2021) 1008–1019, https://doi.org/10.1002/pip.3424.
[21] P. Panek, et al., The new copper composite of pastes for Si solar cells front electrode application, Energy Procedia 92 (2016) 962–970, https://doi.org/10.1016/j.egypro.2016.07.108.
[22] B.H. Teo, et al., Development of nanoparticle copper screen printing pastes for silicon heterojunction solar cells, Sol. Energy 189 (2019) 179–185, https://doi.org/10.1016/j.solener.2019.07.055.
[23] W. Lou, et al., Additives-assisted electrodeposition of fine spherical copper powder from sulfuric acid solution, Powder Technol. 326 (2018) 84–88, https://doi.org/10.1016/j.powtec.2017.12.060.
[24] V.M. Maksimović, et al., Characterization of copper powder particles obtained by electrodeposition as function of different current densities, J. Appl. Electrochem. 39 (12) (2009) 2545, https://doi.org/10.1007/s10800-009-9950-y.
[25] G.H. Gökhan Orhan, Effect of electrolysis parameters on the morphologies of copper powder obtained in a rotating cylinder electrode cell, Powder Technol. 201 (2010) 57–63.
[26] M.-Y. Wang, Z. Wang, Z.-C. Guo, Preparation of electrolytic copper powders with high current efficiency enhanced by super gravity field and its mechanism, Trans. Nonferrous Metals Soc. China 20 (6) (2010) 1154–1160, https://doi.org/10.1016/S1003-6326(09)60271-5.
[27] E. Wiechmann, A. Morales, P. Aqueveque, Improving Productivity and Energy Efficiency in Copper Electrowinning Plants. Industry Applications, IEEE Transactions on 46, 2010, pp. 1264–1270, https://doi.org/10.1109/TIA.2010.2049818.
[28] Q.W. Juanqin Xue, Zhaoqi Wang, Shefeng Yi, Function of additives in electrolytic preparation of copper powder, Hydrometallurgy (2006) 154–156.
[29] F.R. Rasoul Khayyam Nekouie, Nasrollah Naseri Joda, Effect of organic additives on synthesis of copper nano powders by pulsing electrolysis, Powder Technol. 237 (2013) 554–561, https://doi.org/10.1016/j.powtec.2012.12.046.
[30] D.N. Nikolić, et al., Comparative morphological and crystallographic analysis of copper powdersobtained under different electrolysis conditions, Trans. Nonferrous Metals Soc. China 29 (6) (2019) 1275–1284, https://doi.org/10.1016/S1003-6326(19)65034-X.
[31] G.M.P. AG, Products: Copper Powder [cited 2022 02.20.2022]; Available from: https://www.ggp-metal.com/en/.
[32] International, K, Products: Copper Powder, 02 20 [cited 2022 02.20.2022]; Available from: https://www.kymerainternational.com/product_cat/copper/, 2022.
[33] Pometon, Products: Copper Powder [cited 2022 02.20.2022]; Available from: https://www.pometon.com/en/.
[34] Alibaba.com, Alibaba.com, Suoyi New Material Technology Company, 2022.
[35] J.L. Johnson, 20 - Metal injection molding (MIM) of thermal management materials in microelectronics, in: D.F. Heaney (Ed.), Handbook of Metal Injection Molding (Second Edition), Woodhead Publishing, 2019, pp. 461–498.
[36] W.T. Xia, et al., Effect of flow pattern on energy consumption and properties of copper powder in the electrolytic process, Solid State Phenom. 279 (2018) 77–84, https://doi.org/10.4028/www.scientific.net/SSP.279.77.
[37] S.K. Archana Agrawal, D. Bagchi, V. Kumar, B.D. Pandey, Hydrogen Reduction of Copper Bleed Solution From an Indian Copper Smelter for Producing High purity Copper Powders, 2022.
[38] G. Yao, Z.B. Huo, F.M. Jin, Direct Reduction of Copper Oxide Into Copper Under Hydrothermal Conditions, 2022.
[39] M.S. Wu Songping, Preparation of Micron Size Copper Powder With Chemical Reduction Method, 2022.
[40] B. Swain, et al., Selective recovery of pure copper nanopowder from indium-tin-oxide etching wastewater by various wet chemical reduction process: understanding their chemistry and comparisons of sustainable valorization processes, Environ. Res. 147 (2016) 249–258, https://doi.org/10.1016/j.envres.2016.01.032.
[41] M.H. Abdel-Aziz, Production of Copper Powder From Wastewater Containing CuSO4 and Alcoholic Additives in a Modified Stirred Tank Reactor by Cementation, 2022.
[42] NAGAI, R.T.a.T, Hydrogen Reduction of Spent Copper Electrolyte, 2022.
[43] J.Y. Chang, et al., Preparation and characteristic of ultrafine copper-based powders reduced by a two-step reduction method, Mater. Sci. Forum 1003 (2020) 122–127, https://doi.org/10.4028/www.scientific.net/MSF.1003.122.
[44] A.V.K. Agrawal, B.D. Pandey, K.K. Sahu, A Comprehensive Review on the Hydro Metallurgical Process for the Production of Nickel and Copper Powders by Hydrogen Reduction, 2022.
[45] Powder, C, Products: Copper Powder [cited 2022 02.20.2022]; Available from: http://www.cnpcpowder.com/products/copper/.
[46] S. Yenwiset, T. Yenwiset, Design and construction of water atomizer for making metal powder, JOM 21 (1) (2011) 75–81.
[47] X. Lv, et al., Microstructure and properties of Cu-Cr-Nb alloy powder prepared by argon gas atomization, Adv. Powder Technol. 30 (11) (2019) 2464–2472, https://doi.org/10.1016/j.apt.2019.07.013.
[48] N.B. Dhokey, M.G. W., U.C. Chaudhari, Influence of Water Pressure and Apex Angle on Prediction of Particle Size for Atomization of Copper Powder, 2022.
[49] F.A.E. Persson, Anders Eliasson, Pär Jönsson, Pär Jönsson, Prediction of Particle Size for Water Atomized Metal Powders: Parameter Study, 2022.
[50] S.Y.T. Yenwiset, Design and Construction of Water Atomizer for Making Metal Powder, 2022.
[51] H. Liu, E.J. Lavernia, R.H. Rangel, An analysis of freeze-up phenomena during gas atomization of metals, Int. J. Heat Mass Transf. 38 (12) (1995) 2183–2193, https://doi.org/10.1016/0017-9310(94)00345-V.
[52] H.K. Dean Hackett, Advances in powder atomization capabilities enable a range of new thermal spray applications, Adv. Mater. Process. 159 (04) (2001) 31–35.
[53] Shuichi Hamada, Yoshiyuki Kudo, Toshio Tojo, Preparation and reduction kinetics of uniform copper particles from copper(I) oxides with hydrogen, Coll. Surf. 67 (1992) 45–51.

[54] X. Wang, et al., Time-resolved studies for the mechanism of reduction of copper oxides with carbon monoxide: complex behavior of lattice oxygen and the formation of suboxides, J. Phys. Chem. B 108 (36) (2004) 13667–13673, https://doi.org/10.1021/jp0403660.
[55] M.H. Yamukyan, K.V. Manukyan, S.L. Kharatyan, Copper oxide reduction by hydrogen under the self-propagation reaction mode, J. Alloys Compd. 473 (1–2) (2009) 546–549, https://doi.org/10.1016/j.jallcom.2008.06.031.
[56] C.-H.W. Liu-Ho Chiu, Pee-Yew Lee, Comparison between oxide-reduced and water-atomized copper powders used in making sintered wicks of heat pipe, China Particuol. (2007) 220–224.
[57] T.Y. Chan, M.S. Chuang, S.T. Lin, Injection moulding of oxide reduced copper powders, Powder Metall. 48 (2) (2005) 129–133, https://doi.org/10.1179/003258905X37710.
[58] O.D. Neikov, S.S. Naboychenko, N.A. Yefimov, Editors., Copyright, in: Handbook of Non-Ferrous Metal Powders, Second edition, Oxford, Elsevier, 2019, p. iv.
[59] B. Madavali, et al., Effects of atmosphere and milling time on the coarsening of copper powders during mechanical milling, Powder Technol. 256 (2014) 251–256, https://doi.org/10.1016/j.powtec.2014.02.019.
[60] E. Salur, et al., Effect of ball milling time on the structural characteristics and mechanical properties of nano-sized Y2O3 particle reinforced aluminum matrix composites produced by powder metallurgy route, Adv. Powder Technol. 32 (10) (2021) 3826–3844, https://doi.org/10.1016/j.apt.2021.08.031.
[61] O.D. Neikov, Chapter 2 - mechanical crushing and grinding, in: O.D. Neikov, et al. (Eds.), Handbook of Non-Ferrous Metal Powders, Elsevier, Oxford, 2009, pp. 47–62.
[62] I.Y. Saleem, H.D.C. Smyth, Micronization of a soft material: air-jet and micro-ball milling, AAPS PharmSciTech 11 (4) (2010) 1642–1649, https://doi.org/10.1208/s12249-010-9542-5.
[63] A.K. Galwey, M.E. Brown (Eds.), Chapter 12 Decomposition of carbonates, in Studies in Physical and Theoretical Chemistry, Elsevier, 1999, pp. 345–364.
[64] G.A. El-Shobaky, et al., Thermal decomposition of basic cobalt and copper carbonates, J. Therm. Anal. 46 (6) (1996) 1801–1808, https://doi.org/10.1007/BF01980784.
[65] J.M. Montes, et al., Electrical conductivity of metal powders under pressure, Appl. Phys. A 105 (4) (2011) 935–947, https://doi.org/10.1007/s00339-011-6515-9.
[66] Y.P. Mamunya, et al., Influence of pressure on the electrical conductivity of metal powders used as fillers in polymer composites, Powder Technol. 140 (1) (2004) 49–55, https://doi.org/10.1016/j.powtec.2003.11.010.
[67] D. Dong, et al., Assessing the future environmental impacts of copper production in China: implications of the energy transition, J. Clean. Prod. 274 (2020), 122825, https://doi.org/10.1016/j.jclepro.2020.122825.
[68] Foundation, T.E.M, Circularity Indicators, Available from: https://www.ellenmacarthurfoundation.org, March 2022.
[69] V. Hessel, et al., Quantitative sustainability assessment of flow chemistry–from simple metrics to holistic assessment, ACS Sustain. Chem. Eng. 9 (29) (2021) 9508–9540, https://doi.org/10.1021/acssuschemeng.1c02501.
[70] J. Hong, et al., Life cycle assessment of copper production: a case study in China, Int. J. Life Cycle Assess. 23 (9) (2018) 1814–1824, https://doi.org/10.1007/s11367-017-1405-9.
[71] K.J.J. Kuipers, et al., Assessing environmental implications associated with global copper demand and supply scenarios from 2010 to 2050, Glob. Environ. Chang. 49 (2018) 106–115, https://doi.org/10.1016/j.gloenvcha.2018.02.008.
[72] H.T. Wang, et al., Life cycle assessment of metallic copper produced by the pyrometallurgical technology of China, Mater. Sci. Forum 814 (2015) 559–563, https://doi.org/10.4028/www.scientific.net/MSF.814.559.
[73] X. Song, et al., Identification and assessment of environmental burdens of Chinese copper production from a life cycle perspective, Front. Environ. Sci. Eng. 8 (4) (2014) 580–588, https://doi.org/10.1007/s11783-013-0599-8.
[74] J. Kulczycka, et al., Environmental impacts of energy-efficient pyrometallurgical copper smelting technologies: the consequences of technological changes from 2010 to 2050, J. Ind. Ecol. 20 (2) (2016) 304–316, https://doi.org/10.1111/jiec.12369.
[75] Evolution of Electronic Waste Toxicity: Trends in Innovation and Regulation, 2022, p. 147, https://doi.org/10.1016/j.envint.2016.01.022.
[76] Y. Chen, et al., Impact of technological innovation and regulation development on e-waste toxicity: a case study of waste mobile phones, Sci. Rep. 8 (1) (2018) 7100, https://doi.org/10.1038/s41598-018-25400-0.